30-lens interferometer for high energy X-rays

M. Lyubomirskiy[1, a)], I. Snigireva[1, b)], G. Vaughan[1], V. Kohn[2], S. Kuznetsov[3], V. Yunkin[3] and A. Snigirev[4]

[1]*European Synchrotron Radiation facility (ESRF), CS 40220, 71, av des Martyrs, F-38043, Grenoble, France.*
[2]*National Research Centre "Kurchatov Institute", 123182, Moscow, Russia.*
[3]*Institute of Microelectronics Technology RAS, 142432, Chernogolovka, Russia.*
[4]*Baltic Federal University, 236041, Kaliningrad, Russia.*

[a)] Corresponding author: lyubomir@esrf.fr
[b)] irina@esrf.fr

Abstract. We report a hard X-ray multilens interferometer consisting of 30 parallel compound refractive lenses. Under coherent illumination each CRL creates a diffraction limited focal spot - secondary source. An overlapping of coherent beams from these sources resulting in the interference pattern which has a rich longitudinal structure in accordance with the Talbot imaging formalism. The proposed interferometer was experimentally tested at ID11 ESRF beamline for the photon energies 32 keV and 65 keV. The fundamental and fractional Talbot images were recorded with the high resolution CCD camera. An effective source size in the order of 15 μm was determined from the first Talbot image proving that the multilens interferometer can be used as a high resolution beam diagnostic tool.

INTRODUCTION

The advent of the brilliant high coherent X-ray beams produced by 3rd generation synchrotrons has triggered the rapid development of X-ray refractive optics[1-5] and its applications[6-11]. One of the latest directions in the development of refractive optics is in-line X-ray interferometry[12-15]. Recently proposed bilens interferometer allows generating the interference field with a variable period ranging from tens of nanometres to tens of micrometres[12]. As an evolution of inline bilens system, the six-lens interferometer, consisting of 6 parallel lens arrays, was introduced[13]. Six-lens interferometer gives rise to the increase of the contrast of the interference pattern, and furthermore it leads to a narrowing of the interference fringes. While the bilens system produces a pattern with the interference contrast localized throughout downstream of the interferometer, the multilens forms a more complicated interference field which was described using the Talbot imaging formalism[16].

In order to enlarge the beam acceptance, in this paper we propose a multilens interferometer consisting of 30 parallel arrays of CRLs. The acceptance of the 30-lens interferometer is comparable with the beam size at the ESRF undulator beamline. The optical properties of the interferometer were studied experimentally in the X-ray range from 32 to 65 keV. The interference pattern generated by the interferometer was recorded at fundamental and fractional Talbot distances. The effective source size was measured from the width of the interference fringes.

THE INTERFEROMETER DESCRIPTION

The schematic view of the planar parabolic multilens interferometer is depicted in Fig. 1 (a). The interferometer proposed here is conceptually similar to the six-lens interferometer presented earlier[13], except that it consists of the 30 compound refractive lenses across the beam. Each compound refractive lens focuses the beam at the distance $z_f = F/(1 - F/z_0)$, where $F = R/2N\delta$ is the lens focal length and z_0 is the source-to-lens distance, R is the radius of curvature of one parabolic surface, N is the number of double concave elements in the CRL, δ is the decrement of complex refraction index n. Under coherent illumination each lens generates a coherent, diffraction limited focal spot of size $w_f = 0.44\lambda z_f/A_{eff}$, where λ is the wavelength and $A_{eff} = 0.66(\delta\lambda z_f/\beta)$ is the absorption limited effective aperture of the lens[17]. At a distance $z > z_f A_{int}/A_{eff}$ from the focal plane, where A_{int} is the physical aperture of the interferometer, the cones diverging from secondary sources overlap, and in

Proceedings of the 12th International Conference on Synchrotron Radiation Instrumentation – SRI2015
AIP Conf. Proc. 1741, 040022-1–040022-4; doi: 10.1063/1.4952894
Published by AIP Publishing. 978-0-7354-1398-6/$30.00

this region interference occurs. The interference fringe pattern produced by multilens interferometer can be described using Talbot imaging formalism[16] with the only difference that the classical amplitude grid used in Talbot imaging is replaced by a collection of periodic line sources produced by linear lens arrays separated by the distance d. In case of plane wave illumination the fundamental Talbot image appear at the distance $z_T=d^2/\lambda$, and the fractional Talbot distances denotes as $z_n = z_T/n$, where n is integer. We would like to note that the Talbot distance counted from lens foci and and the foci are reproduced in the Talbot planes and are multiply reproduced in the fractional Talbot planes.

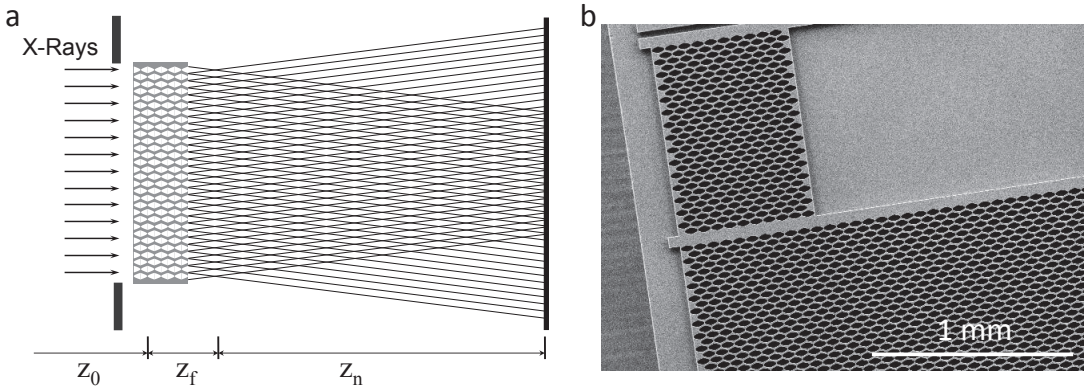

FIGURE 1. (a) Schematic view of the interferometer. (b) Scanning Electron Microscope image of interferometers fabricated in the Si substrate.

The interferometer was manufactured using the electron beam lithography and the deep silicon etching so called the BOSCH process[5]. The Scanning Electron Microscope (SEM) image of 30-lens interferometer is shown in Fig. 1 (b). The longitudinal length and physical aperture of the one individual double concave lens are 62 and 30 μm respectively. The radius of the parabola apex R is 3.75 μm. The lens arrays in the interferometer are arranged in a chessboard pattern, or in other words the arrays are shifted relative to each other by the distance equal to half length of the single lens. The period d of the interferometer across the beam is equal to the physical aperture of single lens, namely, $d = 30$ μm. The beam acceptance of the interferometer is $A_i = 900$ μm (30*30 μm) which coincides with the beam size at 100 meters downstream from the undulator source.

TABLE 1. Parameters of 30 lens interferometers. Diffraction limited resolution calculated for single lens array in the interferometer.

Set number	Energy, keV	Number of lenses	Lens length, μm	Diffraction Limited Resolution, nm	Effective aperture, μm
1	10	10	618	190	13
2	20	39	2416	87	17
3	30	87	5392	63	21
4	40	156	9670	55	23
5	50	243	15064	53	23

With the aim to expand the applicability of the multi-lens interferometers for a wide range of energies, we manufactured five interferometer sets on the same Si chip. They were formally designed for energy range from 10 to 50 keV with 10 keV steps. The focal distance of interferometers for each energy was fixed as $F = 4$ cm that was achieved by varying the number of elementary double concave lenses in CRL arrays of each interferometer. The selection of the proper interferometer set, which is suitable for desired energy, can be performed by parallel displacement of the chip in vertical direction. Table 1 summarized the main parameters of the interferometer sets.

EXPERIMENTAL RESULTS

The experimental tests of the 30-lens interferometer were performed at the long (about 100 m) ID11 ESRF beamline. The monochromatization of the incoming X-rays was performed by the double bent-crystal

monochromator operating in a horizontal Laue geometry. Compared to flat crystals in Bragg geometry, asymmetrically cut bent crystals deliver up to 10 times higher photon flux, particularly at higher energies. The horizontal geometry allows direct crystal cooling via contact with a thermally controlled InGa bath. Attenuators upstream from the monochromator remove essentially all flux below 25 keV; this, coupled with the Laue geometry, means that the thermal load is small and such cooling is sufficient. Consequently, the monochromator is very stable, needing no adjustment or feedback after alignment. The horizontal geometry also minimizes the perturbation of the vertical source size. The source size s was measured by direct imaging using CRL[18] and during the 30-lens interferometer tests it was in order of 15 μm.

The interferometer was mounted on the stage with all necessary rotation and translation movements, allowing alignment in a beam, which was at the distance z_0 = 41.4 m from the source. The registration of the interference patterns was performed by the high resolution X-ray CCD camera equipped with a fluorescence screen and an optical objective which allows one to obtain 3 μm of spatial resolution (1.5 μm pixel size). The quality of the fringes produced by the interferometer can be described quantitatively using the visibility parameter $V = (I_{max} - I_{min})/ (I_{max} + I_{min})$*100%, where, I_{max} and I_{min} are the irradiances corresponding to the maximum and the nearby minimum in the fringe system respectively.

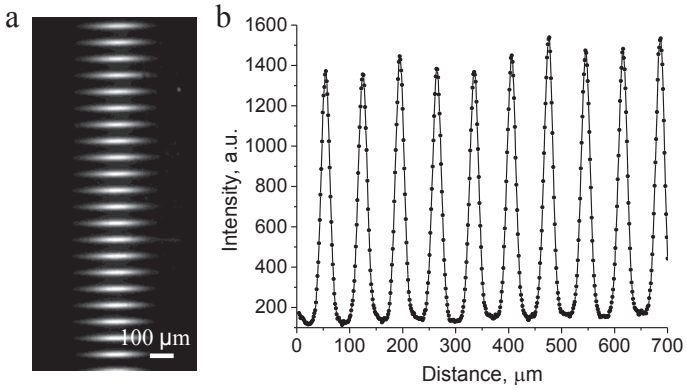

FIGURE 2. (a) An interference pattern generated by the interferometer recorded with 32 keV. (b) The intensity variation obtained for the line though the centre of the fringe pattern, the contrast visibility is approximately 86%.

Taking advantage of ID11 as a long beamline specialized for the high-energies, we studied the multilens interferometer optical properties at 32 and 65 keV X-ray energy recording the fundamental and fractional Talbot images at the distance of about 100 m from the source. Keeping in mind that the observation distance is comparable with the distance to the source, the sphericity of the incident wavefront has to be taken into account. The Talbot images will be magnified by the factor $C_m = (z_f + z_n' + z_0)/(z_0 + z_f)$ and will be located at the distance z_n' which is obtained from the equation:

$$\frac{1}{z_f + z_n'} + \frac{1}{z_0} = \frac{1}{F + z_n} \qquad (1)$$

From the formula (1) it follows that for 32 keV X-rays the fundamental n = 1 Talbot image is located at the distance z_1' = 53 m and has the same period as the object but shifted vertically from the primary image by half a period. The interferometer set #3 consisting of 87 lenses designed for 30 keV was chosen for this experiment.

The registered interference pattern and the intensity variation obtained for the line through the centre of the pattern orthogonal to fringes are shown in Fig. 2. The fringe spacing is d' = 68 μm which corresponds to the theoretical estimation. The interference fringe visibility is 86%. The measured interference fringe FWHM is w_e = 20 μm that corresponds to the projected source size s'. Therefore we can estimate the effective source size as $s = s'z_0/(z_1' + z_f)$ = 15.6 μm that is in a good agreement with the result obtained by direct CRL imaging of the source. It should be noted that for the measured source size the spatial coherence length L_{coh} at the interferometer position is in the order of 110 μm, from which it follows that less than 4 arrays were coherently illuminated. So it proves the validity of our assumption that source size is dominated in the maxima width of the fringe pattern. In the case of the almost diffraction limited sources or full coherent illumination, the convolution of the source size projection and the diffraction limited width of interference fringes has to be done.

In order to demonstrate the applicability of the multilens interferometer at 65 keV, we took the interferometer set #5 with the largest number of lenses, namely, 243. Then the fractional Talbot image with

$n = 2$ which correspond to $z_2' = 53$ m was registered. The registered fringe pattern of the 36 μm spacing and 17% visibility showed full agreement with the calculated values. This result is apparent evidence of the possibility of utilization such interferometer with the extremely high photon energy.

CONCLUSIONS

The 30-lens interferometer for hard X-rays was designed and manufactured. The acceptance of the 30-lens interferometer is comparable with the beam size at the ESRF undulator beamline. The optical properties of the interferometer were studied for the high photon energies up to 65 keV. The first and the second fractional Talbot images were recorded with different irradiation energies. The size of the source was determined from the interference fringe width. The measured value of the source size was in the order of 15 μm and is in full agreement with the result obtained with direct imaging of the source by CRL.

The proposed multilens interferometer can be used as a wavefront diagnostic device in the focusing mode similar to the Shack – Hartmann wavefront sensor[19]. Moreover the wavefront sphericity may be determined from the Talbot images position[20]. In addition one cannot exclude of applying multilens devices as beam conditioning optics for special illumination, projection and beam smoothing at future diffraction-limited SR and XFEL sources.

ACKNOWLEDGMENTS

The work was supported by the Ministry of Science and Education of Russian Federation grants № 14.Y26.31.0002 and № 02.G25.31.0086.

REFERENCES

1. A. Snigirev, V. Kohn, I. Snigireva and B. Lengeler, Nature **384**, 49-51 (1996).
2. B. Lengeler, C. Schroer, J. Tummler, B. Benner, M. Richwin, A. Snigirev, I. Snigireva and M. Drakopoulos, J. Synchrotron Radiat. **6**, 1153-1167 (1999).
3. B. Lengeler, C. G. Schroer, M. Richwin, J. Tümmler, M. Drakopoulos, A. Snigirev and I. Snigireva, Appl. Phys. Letters, **74**, 3924-3926 (1999).
4. V. Aristov, M. Grigoriev, S. Kuznetsov, L. Shabelnikov, V. Yunkin, T. Weitkamp, C. Rau, I. Snigireva, A. Snigirev, M. Hoffmann and E. Voges, Appl. Phys. Letters **77**, 4058-4060 (2000).
5. A. Snigirev, I. Snigireva, M. Grigoriev, V. Yunkin, M. Di Michiel, S. Kuznetsov and G. Vaughan, Proc. SPIE **6705**, (2007), pp. 670506.
6. S. Engemann, H. Reichert, H. Dosch, J. Bilgram, V. Honkimäki and A. Snigirev, Phys. Rev. Lett. **92**, 205701 (2004).
7. M. Drakopoulos, A. Snigirev, I. Snigireva and J. Schilling, Appl. Phys. Letters **86**, 014102 (2005).
8. A. Petukhov, J. Thijssen, D. Hart, A. Imhof, A. Blaaderen, I. Dolbnya, A. Snigirev, A. Moussaid and I. Snigireva, J. Appl. Crystallogr. **39**, 137-144 (2006).
9. A. Bosak, I. Snigireva, K. S. Napolskii and A. Snigirev, Adv. Mater. **22**, 3256-3259 (2010).
10. G. B. M. Vaughan, J. P. Wright, A. Bytchkov, M. Rossat, H. Gleyzolle, I. Snigireva and A. Snigirev, J. Synchrotron Radiat. **18**, 125-133 (2011).
11. P. Ershov, S. Kuznetsov, I. Snigireva, V. Yunkin, A. Goikhman and A. Snigirev, J. Appl. Crystallogr. **46**, 1475-1480 (2013).
12. A. Snigirev, I. Snigireva, V. Kohn, V. Yunkin, S. Kuznetsov, M. B. Grigoriev, T. Roth, G. Vaughan and C. Detlefs, Phys. Rev. Lett. **103**, 064801 (2009).
13. A. Snigirev, I. Snigireva, M. Lyubomirskiy, V. Kohn, V. Yunkin and S. Kuznetsov, Opt. Express **22**, 25842-25852 (2014).
14. M. Lyubomirskiy, I. Snigireva, S. Kuznetsov, V. Yunkin and A. Snigirev, Opt. Lett. **40**, 2205-2208 (2015).
15 A. F. Isakovic, A. Stein, J. B. Warren, A. R. Sandy, S. Narayanan, M. Sprung, J. M. Ablett, D. P. Siddons, M. Metzler and K. Evans-Lutterodt, J. Synchrotron Radiat. **17**, 451-455 (2010).
16. H. F. Talbot, Philos. Mag., 3 **9**, 401-407 (1836).
17. V. G. Kohn, J. Synchrotron Radiat. **19**, 84-92 (2012).
18. T. Weitkamp, O. Chubar, M. Drakopoulos, A. Souvorov, I. Snigireva, A. Snigirev, F. Günzler, C. Schroer and B. Lengeler, Nucl. Instr. Meth. Phys. Res. A **467–468**, 248-251 (2001).
19. S. C. Mayo and B. Sexton, Opt. Lett. **29**, 866-868 (2004).
20. D. Malacara-Doblado, Opt. Eng. **36**, 2016-2024 (1997).